PAPER

Characterization of a high repetition-rate laser-driven short-pulsed neutron source

IOP Publishing Plasma Physics and Controlled Fusion
Plasma Phys. Control. Fusion 60 (2018) 054011 (7pp) https://doi.org/10.1088/1361-6587/aab327

Characterization of a high repetition-rate laser-driven short-pulsed neutron source

J Hah[1,2], J A Nees[1], M D Hammig[2], K Krushelnick[1,2] and A G R Thomas[1,2]

[1] Center for Ultrafast Optical Science, University of Michigan, Ann Arbor, MI 48109 United States of America
[2] Department of Nuclear Engineering and Radiological Sciences, University of Michigan, Ann Arbor, Michigan 48109, United States of America

E-mail: agrt@umich.edu

Received 15 November 2017, revised 16 February 2018
Accepted for publication 1 March 2018
Published 22 March 2018

Abstract

We demonstrate a repetitive, high flux, short-pulsed laser-driven neutron source using a heavy-water jet target. We measure neutron generation at 1/2 kHz repetition rate using several-mJ pulse energies, yielding a time-averaged neutron flux of 2×10^5 neutrons s^{-1} (into 4π steradians). Deuteron spectra are also measured in order to understand source characteristics. Analyses of time-of-flight neutron spectra indicate that two separate populations of neutrons, 'prompt' and 'delayed', are generated at different locations. Gamma-ray emission from neutron capture $^1H(n,\gamma)$ is also measured to confirm the neutron flux.

Keywords: ion acceleration, short-pulse laser, nuclear fusion

(Some figures may appear in colour only in the online journal)

1. Introduction

Intense laser interaction with matter is capable of producing high energy particles and radiation, such as MeV photons, electrons and accelerated ions [1]. For ion acceleration, laser-driven techniques can lead to: (1) a compact system design, (2) low emittance, and (3) short burst durations. These unique characteristics of laser-based ion accelerators allow a variety of potential applications in scientific, medical, and security areas. Since the first measurements of high energy proton acceleration from solid targets in 2000 [2–4], different solid target geometries such as variable target thicknesses or micro-structured surface modifications have been tested to achieve higher energy ion acceleration [5–10]. Targets have been fabricated with small dimensions to increase the density of hot electrons in the target [11, 12]. In spite of better energy conversion efficiency, such mass-limited targets typically require target replacement every shot. Thus, target replacement limits the average flux of energetic ions when high repetition-rate lasers are used. For a high repetition-rate system, a thin tape target or a rotating disk target can be employed [13, 14], providing a fresh target for every shot. However, these methods still suffer from target contamination. For instance, water absorption introduces proton contamination. In addition, when solid targets are irradiated by intense laser pulses, debris from target ablation contaminates optical components inside the chamber and thereby degrades optical performance. Debris can be reduced by replacing conventional thin foil targets with clusters [15–18] or liquid jet/droplet targets [19–23]. Cryogenically cooled D_2 gas jet/cluster targets, which can reduce debris-induced optical degradation, have been tested as acceleration sources for deuterons from which one can drive the DD fusion reaction [15–17]. However, a bulky cooling system is generally required to generate cryogenically cooled targets.

Recently, we developed a room temperature heavy water (D_2O) jet target to accelerate deuterons, resulting in the production of 2.45 MeV of DD-fusion neutrons. This system minimizes debris generation and simplifies the target replacement issue [23]. Forward and backward directed deuteron fluxes were estimated from 2D particle-in-cell (PIC) simulations and were confirmed by time-of-flight (ToF) measurement with scintillation detectors. Hah *et al* also introduced a controlled pre-pulse with an intensity contrast of 10^8 and pre-delay of 13 ns; a target conditioning step that achieved an order of magnitude higher neutron yield. The results

demonstrated the possibility of deploying a compact laser-based neutron source with only several mJ of laser energy per pulse.

In this paper, we further report upon the acceleration of deuterons and the production of fusion neutrons from a heavy water stream target, providing: details of the deuteron cut-off energy and flux; variation of neutron yield with focal position; and confirmation of neutron flux using gamma emission from ^{1}H(n,γ) reactions. By irradiating a room temperature heavy water stream with a high repetition-rate femtosecond laser, we demonstrate a laser-based source producing short duration pulses of neutrons with high average flux. In order to understand the initial neutron angular and energy distribution, the deuteron energy spectra were measured and compared with the detected neutron ToF distribution, which gives the neutron energy distribution.

This paper is structured as follows: In section 2, we describe the laser system, the water target stream generation and detection methods for deuterons and neutrons. Section 3 provides experimental results, including a focal spot scanning experiment, which indicates how the neutron flux is impacted by the focal position relative to the stream. We also discuss measurements using a high purity germanium (HPGe) detector, which measure the gamma-rays resulting from neutron interactions with the surrounding materials and use this to infer the neutron flux. This is compared to previous results and simulations. A summary of the results is given in section 4

2. Experimental setup

The experiment was performed on the Lambda-cubed (λ^3) Ti: Sapphire ($\lambda = 800$ nm) laser facility at the University of Michigan, using laser pulses of duration $\tau = 45 \pm 2$ fs full-width-at-half-maximum (FWHM) with an amplified-spontaneous-emission intensity contrast ratio of 10^8. The λ^3 laser operates at a $1/2$ kHz repetition-rate and delivers up to 18 mJ energy-per-pulse focused on the surface of a heavy water stream target. The laser was focused to a 1.4 μm FWHM focal spot using an $f/1.4$ off-axis parabolic mirror, which produced a maximum peak intensity of 3×10^{19} W cm^{-2} in vacuum. The experimental setup is shown in figure 1. Pre-alignment was conducted manually before evacuating the experimental chamber. After the chamber lid was closed and the chamber pressure decreased, additional post-alignment procedures are required as follows. When laser pulses interact with the water stream, second harmonic light (at 400 nm) is generated and collected by the parabolic mirror, which directs the light out of the chamber. Optimization of second harmonic generation is used to guarantee a normal incidence focus on the stream surface. A cadmium telluride (CdTe) x-ray detector is then used to precisely optimize this alignment to produce the highest average x-ray signal. Fine target alignment is performed using piezo actuators (Newport Picomotor), for *xyz*-control of the paraboloid and the water stream.

An undisturbed 30 μm stream of room temperature D_2O was delivered through a 20 μm diameter capillary via a commercial syringe pump, and allowed to fall into a reservoir. During the experiment, evaporated water filled the chamber to a pressure of 15 Torr, the vapor pressure of water at room temperature. As determined in this work, this *relatively* high pressure not only provided a deuteron catcher but also prevented the target stream from freezing. The deuterium nuclei distributed in the chamber stopped deuterons accelerated from the laser interaction, increasing the overall neutron yield. The effect of different catcher geometries and compositions for DD fusion has been studied both experimentally and computationally [21, 24–28], but it is not necessarily beneficial for the maximization of neutron flux. It rather depends on the target temperature and its corresponding stopping power [25].

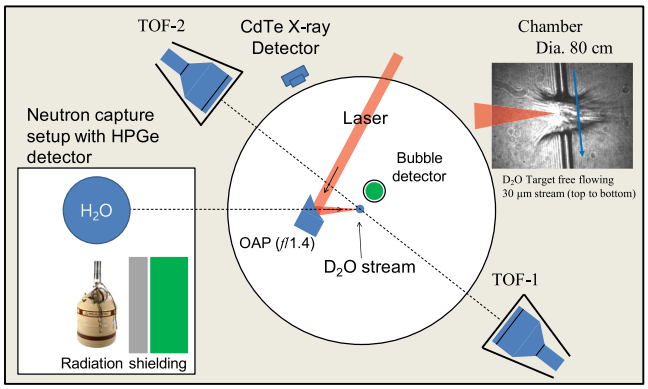

Figure 1. Experimental setup. Image is not to scale. OAP: off-axis parabolic mirror, TOF-1, 2: plastic scintillators with photo-multiplier tubes. Radiation shielding: (green) 10 cm of borated-polyethylene plate and (gray) 5 cm of Pb wall.

2.1. Deuteron spectrum characterization

To measure deuteron acceleration, a CR39 plastic track detector was used with a mylar filter stack. The thin mylar films (each of 2 and 3 μm thickness) were overlaid to obtain different cutoff energies for the deuterons extending up to 840 keV, which corresponds to transmission through an 11 μm thick film. The cutoff energy was calculated using the SRIM software [29]. The exposed CR39 plastic samples were etched with 6.3 molarity NaOH solution for one hour at 90 °C. After the etching, we used an optical microscope to capture images of the region of interest (see figure 2) and ImageJ software to counts ion pits. In this experiment, we located the CR39 detectors at 13.5 and 31 cm away from the water target, a separation necessitated by the limited physical access within the chamber. At these separations, exposure times of 5–10 s result in a roughly optimized number of countable pits that neither oversaturate the detector nor are unduly sparse. The 15 Torr of D_2O vapor inside the chamber provides extra stopping power against accelerated deuterons. At this pressure and distance, the cutoff energy of the mylar filter must be corrected for the deuteron's energy loss in the D_2O vapor. For instance, at 13.5 and 31 cm, the corrected cutoff energy for a 6 μm film is 640 keV and 770 keV, respectively rather than 525 keV. The corrected cutoff energies are tabulated in table 1.

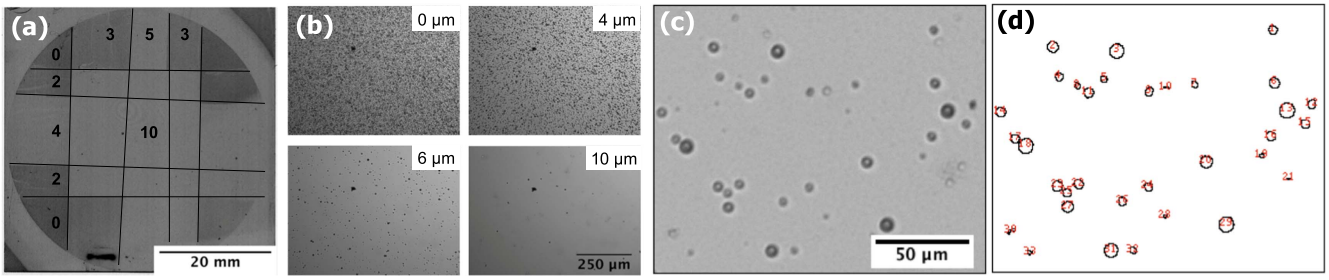

Figure 2. Deuteron ion counts with CR39 detector. (a) A scanned CR39 images of 14 mJ laser pulse with 5 s exposure. A mylar filter stack is applied, and the circular outline is the shadow of the filter holder. The numbers indicate the thickness of the total mylar layers in μm. The central region of the CR39 is covered by a total thickness of 10 μm mylar film. The black lines represent the edges of the filter layers and are added to distinguish the different filter areas. (b) Magnified images of ion pits through different thickness of mylar filter. The number of ion pits is analyzed by the ImageJ software. (c) A magnified raw image of ion pits through 6 μm of mylar filter. (d) Outlines of the ion pit was drawn and counted. A total of 33 ion pits is counted.

Table 1. Calibrated cutoff energies for given mylar film thickness. The latter two columns include corrections for the energy loss in the heavy water vapor.

Thickness (μm)	Uncorrected (keV)	At 13.5 cm (keV)	At 31 cm (keV)
4	375	510	655
6	525	640	770
8	660	760	880
10	780	870	980

Oxygen ions from the target and neutrons may also contribute to extra tracks on the CR39 detector. Using SRIM software, the oxygen stopping distance in mylar is such that to penetrate 4 μm of mylar film and leave a track on the CR39, at least 3.5 MeV kinetic energy is required, which is unlikely. The neutron detection efficiency for DD (2.45 MeV) neutrons on CR39 is $(6.0 \pm 0.7) \times 10^{-5}$ under similar CR39 etch conditions [30], therefore less than 1 neutron-induced track is expected on any one piece of CR39.

2.2. ToF measurements

ToF measurements were made using a plastic scintillator (ELJIN, EJ-204) assembled with a photomultiplier tube (HAMAMATSU, H2431-50); the assembly being wrapped with black tape to block ambient and stray laser light. The tube was negatively biased at 1.8 kV and an oscilloscope recorded the signal. Because strong x-rays were induced by the laser-plasma interactions, the assembly was required a lead (Pb) housing with a thickness of 5 cm surrounding the detector, including the front face. Furthermore, in order to block scattered neutrons, a borated-polyethylene housing covered the assembly, except for the line of sight towards the target. The plastic scintillators were located at 1.95 m (135°) and 3.5 m (−45°) from the laser focus.

2.3. Neutron flux measurement

Two different techniques were employed to measure the neutron flux. First, bubble detectors (Bubble Tech Industries, BD-PND) were placed inside the chamber and exposed to the neutron source for a total of 2 min for each experiment. The bubble detectors were independently calibrated for DD neutrons using a commercial neutron generator at the University of Michigan Neutron Science Laboratory (Thermo Scientific, MP-320). The generator yields 10^6 neutrons per second in the DD neutron-generation mode, and the calibration factor for the bubble detector was 6900 neutrons per bubble. During the measurements, the bubble detectors were covered with a 1 mm thick aluminum tube to avoid direct laser irradiation [23]. The bubble detector has the following advantages: (1) insensitivity to both x-rays and electron interactions, (2) for the model PD-BND employed in the experiment, a flat response across a broad energy range (0.3–10 MeV) [31] and linear bubble generation with respect to neutron flux [32]. Based on these characteristics and the given calibration factor, the neutron flux from the laser-based source can be estimated. Second, gamma-ray emissions from neutron-scatter and neutron-capture reactions in surrounding materials were measured by a cryogenically cooled cylindrical (H 3.27cm × ϕ8.47 cm) HPGe detector (Ortec, GEMPM45P4-108). The detector was located 1.67 m from the target and a shielding wall consisting of 10 cm of borated-polyethylene followed by 5 cm of Pb attenuated the neutron and induced gamma-ray flux as well as the direct x-ray flux incident upon the detector. A water-filled cylindrical container (H 30 cm × ϕ27.5 cm) placed 79 cm from the detector on axis (180°) was exposed to the direct neutron flux, neutrons being (predominantly) captured by hydrogen within the water resulting in a neutron-capture reaction and subsequent gamma-ray emission at 2.22 MeV (^{1}H(n,γ)). The HPGe gamma spectrum was compared with that produced by a Monte Carlo N-particle (MCNP) simulation that included an isotropically emitting neutron source, the water container, and the HPGe detector. The capture-gamma-ray interaction rate within the HPGe detector was derived from both simulated and measured spectra, from which the neutron flux of the source can be estimated.

3. Results and discussion

3.1. Deuteron spectrum characterization

Deuterons were detected by CR39 plastic tract detectors with mylar filter stacks at two different locations (13.5 cm at 30°,

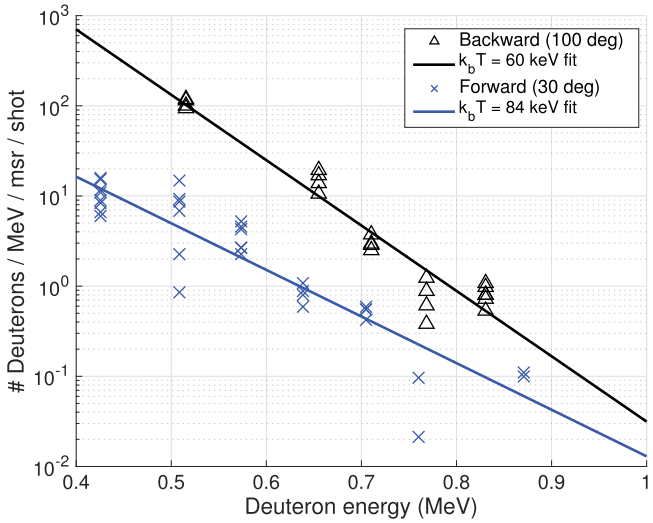

Figure 3. Deuteron energy spectra of forward-directed and backward-directed deuterons derived from CR39 detectors after 5 s laser exposure.

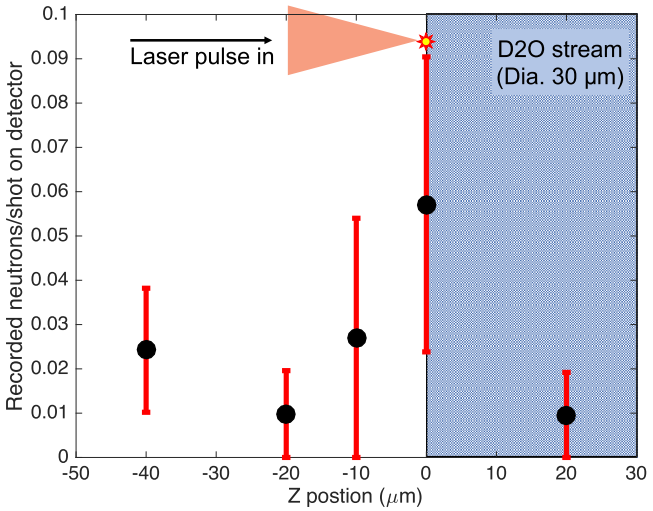

Figure 4. Focal spot scan experiment schematic and results. *Y*-axis shows the number of neutron recorded on the plastic detector per shot. The OAP stage is moved along the laser propagation axis a range from −40 to 20 μm.

and 31 cm at 100°). Figure 2(a) shows one scanned image of a typical CR39 plate. The numbers on the image indicate the thickness of the mylar filter layers in micrometers and the center region has a total mylar thickness of 10 μm. The outer annulus of figure 2(a) is the shadow of the filter holder. In figure 2(b), the microscope images corresponding to propagation through different filter thicknesses are shown. Figures 2(c) and (d) show the results of a 5 s exposure for the detector at 13.5 cm at 30°. ImageJ's analyze particle function was used to count the number of ion pits. Faulty ion signals were rejected by their size and the application of circularity filters. For each region of interest (i.e. different thicknesses of filters), images were randomly captured at 2–8 locations, and analyzed to reduce statistical error. Deuteron spectra are shown in figure 3 in which measured data and fitted curves are plotted. Note that data below 400 keV are not plotted and were excluded for the curve fits because there are too many ion pits to count (e.g. figure 2(b), 0 μm case).

The spectra confirmed that deuterons were accelerated up to the 900 keV level, and the in both forward and backward directions. When comparing the flux above the 400 keV region, it is comparable to the 2D PIC simulation result shown in [23], where 2D PIC simulation showed orders of 10^9 deuterons per shot ($E_D > 100$ keV) in both directions. The backward traveling deuterons (toward vapor side) acted as dominant neutron source.

3.2. Focal axis scanning

During experiments, we examined the neutron flux change as the laser focus was changed along the focal axis. It should be noted that the laser focus is fixed at the $Z = 0$ position except during the focal axis scanning. The OAP was moved by a picomotor within a range from −40 to +20 μm. It should also be noted that when the OAP is moved along the focal axis, its transverse axis was also realigned in order to maximize the radiation flux on the CdTe x-ray detector. Figure 4 shows the results of the focal-spot scan-experiment. For a given set of system parameters, its vacuum *Rayleigh* length is 9 μm, and by retracting the focal point 10 μm, the neutron production rate is scaled to half its maximum value. Also, at −20 μm, the expected beam intensity in vacuum would be 17 % of the peak intensity, which happens to match the neutron production rate. At −40 μm, the corresponding beam intensity should be 5% of the peak intensity, but the neutron flux was about 40% of the peak flux. A possible explanation for this unusual neutron flux could be the result of a beam perturbation in the water-vapor plasma. Another possibility is that the prepulse intensity may dramatically change the scale length of the interaction.

3.3. ToF measurements

The ToF technique was applied to the scintillator traces, typical examples of which are shown in figure 5. In the presence of heavy water, a neutron peak temporally follows the pronounced x-ray peak as shown in a comparison of the red and blue traces. By replacing D_2O with H_2O in the fluidic target system, the generation of DD fusion neutrons can be confirmed. In figure 5, the red trace represents the D_2O result exhibiting a neutron signal (near 100 ns) following after the x-ray peak (near 7 ns); the blue trace (H_2O), however, shows only the x-ray peak. Time zero (i.e. laser-target interaction time) is calculated from the x-ray peak time. The time-of-arrival distribution of the neutron signal is shown in figure 6, in which the histogram has a total of 979 neutron arrival data points and each bin width is 4 ns. It should be noted that the MCNP simulation confirmed that attenuation and scattering of fast neutrons may be ignored for 1.95-meter distance including the vapor and the chamber wall.

A thermal distribution of deuterons broadens the neutron energy spectrum; the gray-colored histogram in figure 6 shows the measured neutron arrival time distribution and the red region indicates the expected neutron signal generated

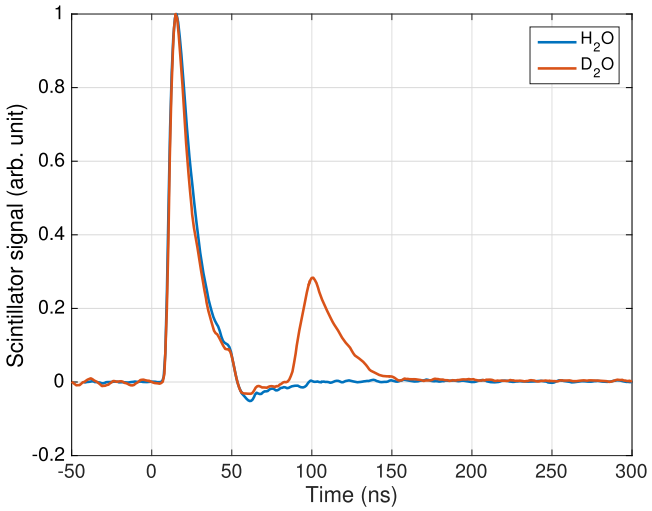

Figure 5. ToF traces from D_2O and H_2O targets for 1.95 m distance. These traces are averaged and normalized with respect to x-ray signals from more than 3000 recorded traces. Both traces show the same response to x-rays. For D_2O, neutrons arrive 90–100 ns after the interaction.

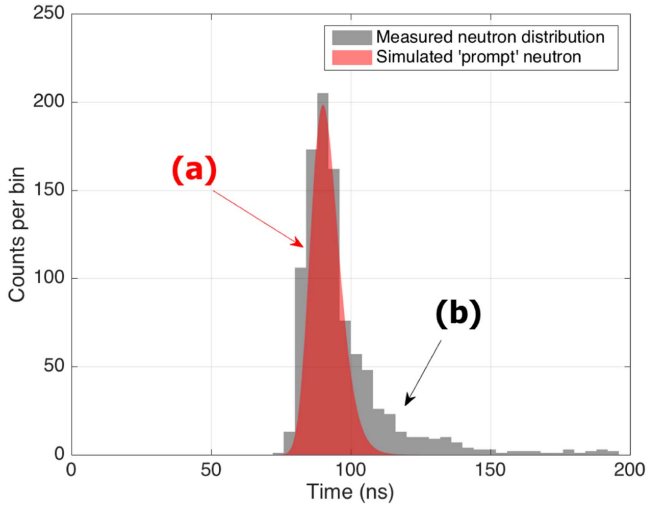

Figure 6. Histogram of neutron arrival times. Total neutron count is 979 from 48000 shots of laser. Approximate neutron detection efficiency of the EJ-204 plastic scintillator is 20%, giving 8×10^4 neutrons s^{-1}. (a) Expected 'prompt' neutron distribution with spectral broadening due to the thermal distribution of the deuterons. (b) Tail of 'delayed' neutrons generated in the vapor.

promptly from the laser-water target interaction (2.45 MeV ± 0.32 MeV). This was calculated using the measured deuteron temperature based on a beam fusion mode model [33], $\Delta E_n = 35\sqrt{T_i}$, where T_i is the deuteron characteristic temperature. $T_i = 84$ keV was taken from the measured effective temperature of the forward directed deuterons.

The most probable transit time of the histogram is 90 ns, which corresponds to an energy of 2.45 MeV for a neutron generated at the time of laser interaction ('prompt' neutron) 1.95 m from the detector. For the early arrival neutrons (<90 ns), 497 out of 979 neutrons (50.8%) were detected before 90 ns, which was well matched to the broadened neutron energy spectrum (red area), area below 0–90 ns

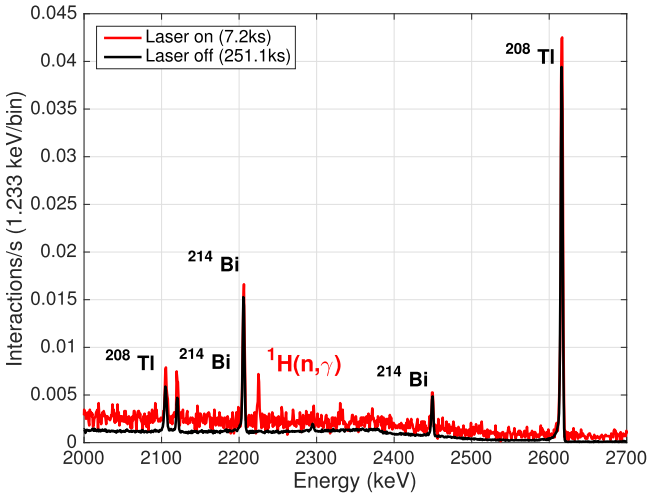

Figure 7. HPGe gamma-ray spectra from 2 to 2.7 MeV showing the difference between the background distribution (in black) and the laser-on distribution (in red). The background was collected for 8 h and the laser-on distribution was collected for 2 h.

region is 50.7%. For the late arrival neutrons (>90 ns), the measured neutron arrival times were lengthened more than the broadening of the neutron spectrum due to the deuteron energy distribution (see figure 6(b)), which can reduce the neutron lower energy to 1.56 MeV (113 ns in ToF). The measured data showed that 11% neutrons arrived after 113 ns. These 'delayed' neutrons can be explained by the backward directed deuterons that interact with the vapor. Due to the low density of the vapor, the deuteron stopping distance is significantly extended (from a few cm to a few μm). This extra deuteron transit time is a few tens of ns. These escaped deuterons generate fusion reactions which could take place through the entire chamber volume, leading to a delay of ToF signals. The spread of ToF signals also was observed by Karsch *et al* [21], who employed catcher to catches ions from both front and rear surfaces of water droplets. Here, a self-generated D_2O vapor catcher stops the accelerated deuterons throughout the chamber and one does not, therefore, observe clear secondary neutron peaks at a highly localized catcher location.

3.4. Neutron flux

Previously, we estimated and scaled the neutron flux of the system by using a bubble detector and 2D PIC simulations [23]. Here, we employed an HPGe detector to confirm the neutron flux. Figure 7 and 8 shows gamma spectra collected during the experiments. The background gamma-ray distribution of the laboratory was collected for 8 h and compared with the results from a 2 h long laser operation. The two spectra are normalized with respect to the live-time of the measurement and the energy axis is calibrated from 14 lines in the background. At 2.22 MeV, a proton–neutron capture gamma signal grows in intensity with a constant rate across the 2 hour experiment. From the MCNP simulation, the 2.22 MeV neutron capture gamma from hydrogen is the predominant feature regardless of the neutron source (DD or

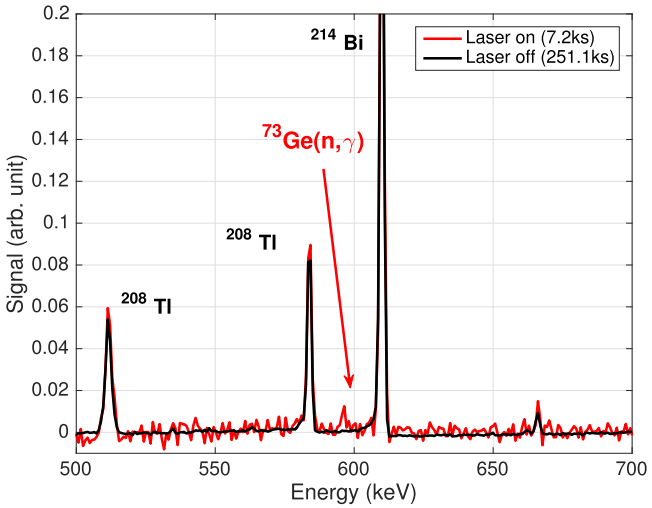

Figure 8. HPGe gamma-ray spectra from 0.5 to 0.7 MeV showing the difference between the background distribution (in black) and the laser-on distribution (in red). The background was collected for 8 h and the laser-on distribution was collected for 2 h. The baseline of the background distribution was removed to clarify the appear of the germanium capture peak.

DT). Because the deuteron energy extends only up to 1 MeV (see section 3.1), neutrons from these deuterons are isotropically emitted [24, 34]. When simulating the configuration (DD neutron source, water bath, and HPGe detector at each position), 1.59×10^9 neutrons from the isotropic source are required to generate the 86 ^{1}H(n,γ) counts in the distribution, which given the measurement time, results in 2.2×10^5 neutron per second into 4π sr.

From the simulation, the second most prominent gamma-ray line is at 596.4 keV (^{73}Ge(n,γ)), which is the nuclear emission following the neutron capture by ^{73}Ge within the detector itself. Although the borated polyethylene and lead shielding reduces the direct neutron exposure upon the HPGe detector, unattenuated and scattered neutrons (from the shielding, the water container target, and surrounding material) can thermalize and interact within the detector, as confirmed with simulations that include the shielding configuration (see figure 8). For those neutrons that have a direct path to the detector, 99.9% of 2.45 MeV DD neutrons travel through the vapor-filled-chamber without losing their energies, and among them, 36.5% of neutrons still have 2.45 MeV energy after 5 cm of thick Pb housing. A 5 cm borated polyethylene shield reduce the number of unattenuated 2.45 MeV neutrons by 77.6%.

4. Conclusion

In conclusion, we have demonstrated the production of a short-pulsed source of fast neutrons via laser-plasma deuteron acceleration and their subsequent DD fusion reactions using a multi-mJ, fs duration pulsed laser system operating at a high repetition-rate (1/2 kHz). The deuteron energy spectra were measured in two directions using mylar filter stacks. In both directions, deuteron energies were measured up to 0.9 MeV, with the total number of deuterons above 0.4 MeV comparable to that yielded in a 2D PIC simulation [23]. Without an extra pitcher-catcher arrangement, accelerated deuterons collide with deuterium nuclei in the heavy water stream ('prompt') and vapor in the chamber ('delayed'), yielding a 2.45 ± 0.32 MeV energy neutron flux of 2.2×10^5 per second. The neutron average flux is comparable to other laser-based neutron sources [15, 17, 35–39], but our neutron source only requires a few mJ of pulse energy, achieved without a bulky and complex cryogenic target cooling system.

Acknowledgments

This material is based upon the work supported by the Air Force Office of Scientific Research Young Investigator Program under Award No. FA9550-12-1-0310, and partially supported by the Air Force Office of Scientific Research under Award No. FA9550-14-1-0282, and also is supported by the US Department of Energy Grant No. DE-NA0002372 and the US Army Contract No. W15QKN-12-C-0047. JAN would like to acknowledge helpful collaboration with the group of Dr. Roquemore at AFRL, Dayton, OH.

ORCID iDs

J Hah https://orcid.org/0000-0001-5349-0988
J A Nees https://orcid.org/0000-0001-8277-9123
M D Hammig https://orcid.org/0000-0003-1661-9185
K Krushelnick https://orcid.org/0000-0001-9116-9511
A G R Thomas https://orcid.org/0000-0003-3206-8512

References

[1] Borghesi M 2014 *Proc. 1st European Advanced Accelerator Concepts Workshop 2013; Nucl. Instrum. Methods Phys. Res.* A **740** 6–9
[2] Clark E L *et al* 2000 *Phys. Rev. Lett.* **84** 670–3
[3] Maksimchuk A, Gu S, Flippo K, Umstadter D and Bychenkov V Y 2000 *Phys. Rev. Lett.* **84** 4108–11
[4] Snavely R A *et al* 2000 *Phys. Rev. Lett.* **85** 2945–8
[5] Murakami Y, Kitagawa Y, Sentoku Y, Mori M, Kodama R, Tanaka K A, Mima K and Yamanaka T 2001 *Phys. Plasmas* **8** 4138–43
[6] Schwoerer H, Pfotenhauer S, Jackel O, Amthor K U, Liesfeld B, Ziegler W, Sauerbrey R, Ledingham K W D and Esirkepov T 2006 *Nature* **439** 445–8
[7] Chen M, Pukhov A, Yu T P and Sheng Z M 2009 *Phys. Rev. Lett.* **103** 024801
[8] Andreev A A, Steinke S, Sokollik T, Schnürer M, Avetsiyan S T, Platonov K Y and Nickles P V 2009 *Phys. Plasmas* **16** 013103
[9] Klimo O, Psikal J, Limpouch J, Proska J, Novotny F, Ceccotti T, Floquet V and Kawata S 2011 *New J. Phys.* **13** 053028
[10] Khaghani D *et al* 2017 *Sci. Rep.* **7** 11366
[11] Richardson M, Torres D, DePriest C, Jin F and Shimkaveg G 1998 *Opt. Commun.* **145** 109–12

[12] Myatt J, Theobald W, Delettrez J A, Stoeckl C, Storm M, Sangster T C, Maximov A V and Short R W 2007 *Phys. Plasmas* **14** 056301
[13] Nayuki T, Oishi Y, Fujii T, Nemoto K, Kayoiji T, Okano Y, Hironaka Y, Nakamura K G, Kondo K I and Ueda K I 2003 *Rev. Sci. Instrum.* **74** 3293–6
[14] Hou B, Easter J, Krushelnick K and Nees J A 2008 *Appl. Phys. Lett.* **92** 161501
[15] Ditmire T, Zweiback J, Yanovsky V, Cowan T, Hays G and Wharton K 1999 *Nature* **398** 489–92
[16] Zweiback J, Smith R A, Cowan T E, Hays G, Wharton K B, Yanovsky V P and Ditmire T 2000 *Phys. Rev. Lett.* **84** 2634–7
[17] Fritzler S, Najmudin Z, Malka V, Krushelnick K, Marle C, Walton B, Wei M S, Clarke R J and Dangor A E 2002 *Phys. Rev. Lett.* **89** 165004
[18] Grillon G *et al* 2002 *Phys. Rev. Lett.* **89** 065005
[19] Rymell L and Hertz H 1993 *Opt. Commun.* **103** 105–10
[20] Malmqvist L, Rymell L, Berglund M and Hertz H M 1996 *Rev. Sci. Instrum.* **67** 4150–3
[21] Karsch S, Düsterer S, Schwoerer H, Ewald F, Habs D, Hegelich M, Pretzler G, Pukhov A, Witte K and Sauerbrey R 2003 *Phys. Rev. Lett.* **91** 015001
[22] Ter-Avetisyan S, Schnürer M, Hilscher D, Jahnke U, Busch S, Nickles P V and Sandner W 2005 *Phys. Plasmas* **12** 012702
[23] Hah J, Petrov G M, Nees J A, He Z H, Hammig M D, Krushelnick K and Thomas A G R 2016 *Appl. Phys. Lett.* **109** 144102
[24] Davis J, Petrov G M, Petrova T, Willingale L, Maksimchuk A and Krushelnick K 2010 *Plasma Phys. Control. Fusion* **52** 045015
[25] Willingale L *et al* 2011 *Phys. Plasmas* **18** 083106
[26] Zulick C *et al* 2013 *Appl. Phys. Lett.* **102** 124101
[27] Maksimchuk A, Raymond A, Yu F, Petrov G M, Dollar F, Willingale L, Zulick C, Davis J and Krushelnick K 2013 *Appl. Phys. Lett.* **102** 191117
[28] Kar S *et al* 2016 *New J. Phys.* **18** 053002
[29] Ziegler J F, Ziegler M and Biersack J 2010 *Nucl. Instrum. Methods Phys. Res.* B **268** 1818–23
[30] Frenje J A *et al* 2002 *Rev. Sci. Instrum.* **73** 2597–605
[31] Gherendi M *et al* 2008 *J. Optoelectron. Adv. Mater.* **10** 2092–4
[32] Ing H 2001 *Radiat. Meas.* **33** 275–86
[33] Kitagawa Y *et al* 2011 *Plasma Fusion Res.* **6** 1306006
[34] Davis J and Petrov G M 2008 *Plasma Phys. Control. Fusion* **50** 065016
[35] Pretzler G *et al* 1998 *Phys. Rev.* E **58** 1165–8
[36] Yang J M *et al* 2004 *J. Appl. Phys.* **96** 6912–8
[37] Lancaster K L *et al* 2004 *Phys. Plasmas* **11** 3404–8
[38] Žagar T, Galy J, Magill J and Kellett M 2005 *New J. Phys.* **7** 253
[39] Giulietti D *et al* 2017 *Europhys. Lett.* **119** 65001